Journal of Sound and Vibration (1996) **194**(2), 243–263

PERIODIC RESPONSE OF MECHANICAL SYSTEMS WITH LOCAL NON-LINEARITIES USING AN ENHANCED GALERKIN TECHNIQUE

T. J. ROYSTON† and R. SINGH

Acoustics and Dynamics Laboratory, Department of Mechanical Engineering, The Ohio State University, Columbus, OH 43210-1107, *U.S.A.*

(*Received* 16 *November* 1994 *and in final form* 22 *November* 1995)

A new semi-analytical framework for the study of mechanical systems with local non-linearities is presented. It recognizes that many practical built-up structures consist of non-linearities, typically at joints or junctions, with a few degrees-of-freedom, coupled with many linear degrees-of-freedom of the adjoining components. Unlike linear systems, sinusoidal excitation produces a periodic response, including super and subharmonics. A Galerkin based computational method for the solution of the steady state periodic response of mechanical systems with local non-linearities, defined in the time and/or frequency domains, is proposed. The method incorporates a form of order reduction and numerical continuation with distinct benefits. Order reduction enables inclusion of the extensive and necessary, but often linear, assembled component dynamics with minimal computational cost. Additionally, the proposed form of reduction allows non-linearities explicitly defined in the frequency and the time domain to be handled simultaneously. The continuation scheme, based on the QR decomposition, facilities parametric studies for design by using the system solution for one set of parameters to optimally predict the steady state periodic solution for a similar set of parameters. Two specific examples have been chosen to illustrate the key concepts and methodology of the dual domain method. In the first example, a rigid body connected to a simply supported elastic beam via a non-linear spring is considered. The hydraulic engine mounting system is presented as the second example; a practical representative of the issues discussed in this article. Results of digital and analog computational studies verify the accuracy of the proposed method and highlight its unique capabilities.

© 1996 Academic Press Limited

1. INTRODUCTION

Local non-linearities exist in many physical systems, machines and structures, often at the joints or junctions of assembled components. These non-linearities may be intentionally designed to meet specific performance requirements or may occur due to manufacturing tolerances and wear.

For the sake of illustration, consider the built-up assembly of Figure 1 which consists of two components or subsystems, (1) and (2), that are connected via an element or joint containing a local non-linearity (J). The subsystems, with potentially large numbers of degrees-of-freedom, may represent machine or structural components or subassemblies such as shafts, panels, casings, base supports, or other equipment. The dynamic response

† Present address: Department of Mechanical Engineering, The University of Illinois at Chicago, Chicago, IL 60607-7022, USA.

0022–460X/96/270243 + 21 $18.00/0 © 1996 Academic Press Limited

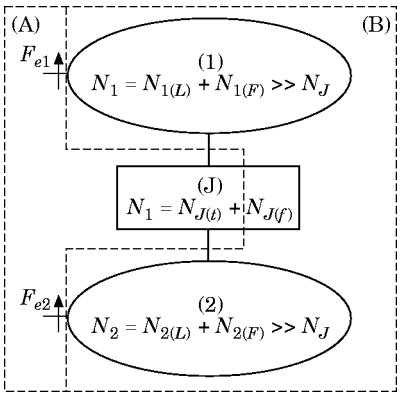

Figure 1. Built-up structure with local non-linearity at junction. Here, N_1 and N_2 refer to the number of linear-degrees-of-freedom in components (1) and (2), and N_J refers to the number of non-linear-degrees-of-freedom in the junction (J). Also, $F_{e1,2}$ denote external force inputs; subscripts t and f indicate whether a non-linear-degree-of-freedom is defined in the time or frequency domain; subscripts F and L indicate whether a linear-degree-of-freedom is or is not associated with an external force input.

in these subsystems is often reasonably approximated with linear relationships. The subsystems are connected together at a junction or joint element which may itself possess N_J-degrees-of-freedom. There may exist abrupt changes in material properties or geometry, friction, or fluid processes at this junction, resulting in a local non-linearity. Consequently, the overall dynamics of an extensive but otherwise linear system may be influenced by non-linear constraints or relationships.

For such problems, the direct time domain integration approach is often employed for non-linear simulation; but, it is computationally inefficient, especially when extensive parametric and design studies need to be conducted for a dynamic system of very high dimension. Also, numerical simulations may not lead to an improved understanding of the non-linear dynamic behavior. Therefore, semi-analytical methods must be utilized. The selection of a particular analysis method is influenced by the nature of excitation and response in addition to the types of non-linearities to be considered. In this paper, it is assumed that periodic (or multi-harmonic) excitation exists in the presence of time-invariant (static) loads which may alter the static equilibrium positions of localized springs and dampers. Only the steady state periodic vibration response including sub and superhamonics are of interest. Finally, it is anticipated that non-linear interactions may be strong in some cases.

2. LITERATURE REVIEW AND OBJECTIVES

Several analytical or semi-analytical approaches are available in the literature [1–20]. A brief review of their applicability to the problem stated above is as follows. Many analytical perturbation techniques [1] assume weak non-linear interactions. The single term harmonic balance or the describing function method [1-4] can handle strong non-linear interactions, but calculates the response only at one frequency. An analytical multi-term harmonic balance can become quite cumbersome for large order systems with many harmonics of interest. Because of such limitations, these analytical methods may be insufficient for the problem considered in this study.

Semi-analytical versions of the harmonic balance method such as the incremental harmonic balance [5, 6], trigonometric collocation [7–9], alternating

frequency/time [10–13], and Galerkin method of weighted residuals [14–19], having many similarities between them, appear to be well suited to systems where a multi-harmonic response to single or few harmonic excitation is present. Of these methods, the Galerkin approach may be the most appealing due to the fact that there exists a clear theoretical framework to answer questions of existence, error bounds, and stability of solutions [14–16]. Also well suited to such problems is the shooting method [20], where essentially the system equations are numerically integrated over the assumed fundamental period of the response and initial state variable values which yield a steady state periodic response (initial and ending values match) are found iteratively by using a Newton-Raphson or comparable technique.

However, in spite of improvements in efficiency over the direct time integration techniques, application of these methods to non-linear systems with many degrees-of-freedom is still computationally complex and time consuming. But often, non-linearities in a real-life physical system are highly localized, present only in a small number of degrees-of-freedom. The obvious approach to such problems is to use non-linear techniques for the non-linear degrees-of-freedom, while employing much simpler linear system methods on the linear degrees-of-freedom. In other words, one should incorporate some sort of linear order reduction into the solution strategy. While a way of accomplishing this using the shooting techniques is not readily apparent, a few investigators have already demonstrated its feasibility in the semi-analytical harmonic balance methods [7, 8, 11].

Finally, incorporation of a continuation or parameter path following technique into the solution process is very desirable as such a technique could make the parametric and design study of complex systems more efficient. A technique employing QR decomposition has been incorporated into the Galerkin method in reference [17], and one employing a Euler-Newton arclength strategy has been applied to the shooting method in reference [20]. Use of the QR decomposition approach in many cases may be more desirable as it tends to produce more uniform steps along the solution curve and it may be more robust.

An optimal combination of all the above-mentioned strategies is needed, which is indeed the main objective of this paper. Specifically, a computational Galerkin method for solution of the steady state periodic response of nonlinear systems is enhanced with a form of order reduction and numerical continuation. A dual domain approach is presented which allows nonlinearities to be defined in the time and/or frequency domain. Order reduction enables a large number of linear degrees of freedom to be efficiently handled. Continuation facilitates parametric studies for design by capitalizing on the steady state solution of the system for one set of parameters in finding its solution for a similar set of parameters, or even excitation amplitudes and frequencies. Computational studies of two specific examples are used to verify the accuracy of the proposed method and highlight its unique capabilities.

3. NON-LINEAR SOLUTION STRATEGY: ENHANCED GALERKIN TECHNIQUE

3.1. THE CONVENTIONAL GALERKIN METHOD

The system of Figure 1 can be substructured into two sections as shown in Figure 2. Section (A) contains the degrees-of-freedom with non-linearities defined in the time domain and degrees-of-freedom driven by external forces. Section (B) contains all remaining linear degrees-of-freedom and degrees-of-freedom with non-linearities defined in the frequency domain.

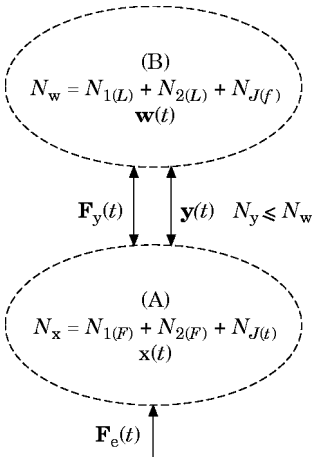

Figure 2. Subsystem structuring approach. Here, N_y denotes the dimension of the force/displacement connection between Sections (A) and (B).

Applying the Galerkin method, the equations of motion can be written as $N_x + N_w$ coupled second order differential equations:

$$\mathbf{d}^{\mathbf{x}}(t) \equiv \mathbf{X}[\mathbf{x}(t), \mathbf{w}(t), \dot{\mathbf{x}}(t), \dot{\mathbf{w}}(t), t] - \ddot{\mathbf{x}}(t) = \mathbf{0}, \qquad \mathbf{d}^{\mathbf{x}} \equiv [\mathrm{d}^{x_1}, \mathrm{d}^{x_2}, \ldots, \mathrm{d}^{x_{N_x}}]^{\mathrm{T}}, \tag{1a}$$

$$\mathbf{d}^{\mathbf{w}}(t) \equiv \mathbf{W}[\mathbf{x}(t), \mathbf{w}(t), \dot{\mathbf{x}}(t), \dot{\mathbf{w}}(t), t] - \ddot{\mathbf{w}}(t) = \mathbf{0}, \qquad \mathbf{d}^{\mathbf{w}} \equiv [\mathrm{d}^{w_1}, \mathrm{d}^{w_2}, \ldots, \mathrm{d}^{w_{N_w}}]^{\mathrm{T}},$$

$$\mathbf{x} \equiv [x_1, x_2, \ldots, x_{N_x}]^{\mathrm{T}}, \qquad \mathbf{w} \equiv [w_1, w_2, \ldots, w_{N_w}]^{\mathrm{T}}, \tag{1b}$$

where $\cdot \equiv \partial/\partial t$, $\cdot\cdot \equiv \partial^2/\partial t^2$ and superscript T denotes the transpose. Consider periodic excitation with fundamental excitation frequency ω. Then, $\mathbf{x}$ and $\mathbf{w}$ will be periodic with base period $m(2\pi/\omega)$ where m is the highest order subharmonic of ω assumed in the response. (Refer to Appendix A.1 for the identification of symbols.) By selecting a suitable non-dimensional time variable $\tau = \omega t/m$, the problem is reformulated with

$$\mathbf{d}^{\mathbf{X}}(\tau) = \mathbf{0}, \qquad \mathbf{d}^{\mathbf{w}}(\tau) = \mathbf{0}, \tag{2a,b}$$

and now $\mathbf{x}$ and $\mathbf{w}$ are periodic with fundamental period 2π. The mnth approximate solution incorporating m subharmonics and n superharmonics of ω can be expressed as truncated series:

$$\mathbf{x}^{mn}(\tau) = \mathbf{a}_0^{\mathbf{x}} + \sum_{k=1}^{mn} \mathbf{a}_{2k-1}^{\mathbf{x}} \sin(k\tau) + \mathbf{a}_{2k}^{\mathbf{x}} \cos(k\tau), \qquad \mathbf{a}_k^{\mathbf{x}} \equiv [a_k^{x_1}, a_k^{x_2}, \ldots, a_k^{x_{N_x}}]^{\mathrm{T}}, \tag{3a}$$

$$\mathbf{w}^{mn}(\tau) = \mathbf{a}_0^{\mathbf{w}} + \sum_{k=1}^{mn} \mathbf{a}_{2k-1}^{\mathbf{w}} \sin(k\tau) + \mathbf{a}_{2k}^{\mathbf{w}} \cos(k\tau), \qquad \mathbf{a}_k^{\mathbf{w}} \equiv [a_k^{w_1}, a_k^{w_2}, \ldots, a_k^{w_{N_w}}]^{\mathrm{T}}. \tag{3b}$$

By substituting equations (3a,b) into equations (2a,b) and numerically calculating the Fourier coefficients of $\mathbf{d}^{\mathbf{x}^{mn}}(\tau)$ and $\mathbf{d}^{\mathbf{w}^{mn}}(\tau)$, one obtains the following determining equations for the coefficients $\boldsymbol{\alpha}^{\mathbf{x}} \equiv [\mathbf{a}_0^x\ \mathbf{a}_1^x \cdots \mathbf{a}_{4mn}^x]$ and $\boldsymbol{\alpha}^{\mathbf{w}} \equiv [\mathbf{a}_0^w\ \mathbf{a}_1^w \cdots \mathbf{a}_{4mn}^w]$:

$$\mathbf{D}_j^{\mathbf{x}^{mn}}(\boldsymbol{\alpha}) \equiv \mathscr{F}_j[\mathbf{d}^{\mathbf{x}^{mn}}(\tau)] = \mathbf{0}, \qquad \mathbf{D}_j^{\mathbf{w}^{mn}}(\boldsymbol{\alpha}) \equiv \mathscr{F}_j[\mathbf{d}^{\mathbf{w}^{mn}}(\tau)] = \mathbf{0}, \qquad j = 0, \ldots, 4nm, \tag{4a,b}$$

where

$$\boldsymbol{\alpha} \equiv [\boldsymbol{\alpha}^{x}\ \boldsymbol{\alpha}^{w}]^{T}, \qquad \mathscr{F}_0[\mathrm{d}(\tau)] \equiv \frac{1}{2P}\sum_{\mathrm{p}=1}^{2P} \mathrm{d}(\tau_{\mathrm{p}}), \qquad \mathscr{F}_{2k-1}[\mathrm{d}(\tau)] \equiv \frac{1}{P}\sum_{p=1}^{2P} \mathrm{d}(\tau_p)\sin(k\tau_p),$$

$$\mathscr{F}_{2k}[\mathrm{d}(\tau)] \equiv \frac{1}{P}\sum_{p=1}^{2P} \mathrm{d}(\tau_{\mathrm{p}})\cos(k\tau_p), \qquad k = 1, \ldots, 2nm,$$

and

$$\tau_p = \frac{(2p-1)}{2P}\pi, \qquad \text{with } P \geqslant 2nm, \qquad p = 1, \ldots, P.$$

Thus one has $N = (4nm + 1) \times (N_x + N_w)$ coupled non-linear algebraic equations for calculating $\boldsymbol{\alpha}$. Solution of these equations is only equivalent to solving the system differential equations in an "average" sense. While a "strong" form solution must satisfy the governing differential equations (2a,b) at all points in time, this "weak" form solution, manifested in equations (4a,b), satisfies weighted integrals or residuals of the governing differential equation over time. These weighted integrals, Fourier transforms in this case, produce agreement in magnitude and phases between the strong and weak solutions in the frequency domain at the selected $2nm + 1$ discrete frequencies (including the d.c. component). If the system response is dominated by components at these frequencies (a fundamental assumption of the technique), then the "weak" form or orthogonal solution will agree excellently with the "strong" form solution. Another issue worth mentioning is that use of the discrete representation of the Fourier transform (DFT) in place of the continuous integral form (which technically makes this a collocation method) does not affect computations in a practical manner since both forms of the transform should yield identical results in the absence of aliasing.

An interative method must be employed to solve the coupled non-linear algebraic equations. A suitable scalar residual R to be minimized is the sum of the squares of the determining equations in the frequency domain:

$$R = \sum_{j=0}^{4nm}\left\{\sum_{s=1}^{N_x}\left|D_j^{x^{mn}}\right|^2 + \sum_{s=1}^{N_w}\left|D_j^{w^{wn}}\right|^2\right\}. \tag{5}$$

Note that while only $nm + 1$ frequencies are used in the approximate solutions, $\mathbf{x}^{mn}$ and $\mathbf{w}^{mn}$ of equations (3a,b), $2nm + 1$ frequencies are used in the calculation of R. Hence, the truncation error is accounted for as well [19]. Proof of the convergence of the Galerkin method can be found in reference [16]. Also, in reference [14], it is shown that for cases which can be cast in an equivalent variational form, the convergence properties associated with the Raleigh-Ritz method carry over to the Galerkin method.

3.2. SOLUTION VIA QR DECOMPOSITION AND CONTINUATION

The QR decomposition is employed in a Newton-Raphson based continuation strategy to efficiently solve equations (4a,b) while satisfying equation (5) for a range of values of Ω, which could represent any system design parameter, like a spring stiffness or viscous damping coefficient, or external variables like the amplitude or fundamental frequency of the periodic excitation force. A continuous smooth curve of solutions in the $N + 1$ dimensional space spanned by the coefficients $\boldsymbol{\alpha}$ and system parameter Ω will exist if the governing equations (2a,b) are infinitely differentiable. The iterative strategy involves alternating between two tasks: (1) converging to a point on the solution curve, and (2) from

that point, estimating a nearby point on the curve. The Newton-Raphson based method can be expressed in the following form for the ith iteration:

$$\mathbf{J}_a\boldsymbol{\Delta} + \mathbf{D} = \mathbf{0} \quad \text{where } \boldsymbol{\Delta} \equiv \begin{bmatrix} \boldsymbol{\alpha}^{(i+1)} - \boldsymbol{\alpha}^{(i)} \\ \Omega^{(i+1)} - \Omega^{(i)} \end{bmatrix}, \qquad \mathbf{D} \equiv \begin{bmatrix} \mathbf{D}^{\mathbf{x}} \\ \mathbf{D}^{\mathbf{w}} \end{bmatrix},$$

$$\mathbf{D}^{\mathbf{x}} \equiv [\mathbf{D}_0^{x^{mn}} \cdots \mathbf{D}_{4_{nm}}^{x^{mn}}]^{\mathrm{T}}, \qquad \mathbf{D}^{\mathbf{w}} \equiv [\mathbf{D}_0^{w^{mn}} \cdots \mathbf{D}_{4_{nm}}^{w^{mn}}]^{\mathrm{T}},$$

and

$$\mathbf{J}_a \equiv \left[\mathbf{J}\,\frac{\partial \mathbf{D}}{\partial \Omega}\right] \equiv \begin{bmatrix} \dfrac{\partial \mathbf{D}^{\mathbf{x}}}{\partial \boldsymbol{\alpha}^{\mathbf{x}}} & \dfrac{\partial \mathbf{D}^{\mathbf{x}}}{\partial \boldsymbol{\alpha}^{\mathbf{w}}} & \dfrac{\partial \mathbf{D}^{\mathbf{x}}}{\partial \Omega} \\ \dfrac{\partial \mathbf{D}^{\mathbf{w}}}{\partial \boldsymbol{\alpha}^{\mathbf{x}}} & \dfrac{\partial \mathbf{D}^{\mathbf{w}}}{\partial \boldsymbol{\alpha}^{\mathbf{w}}} & \dfrac{\partial \mathbf{D}^{\mathbf{w}}}{\partial \Omega} \end{bmatrix}. \tag{6}$$

Here, $\mathbf{J}$ and $\mathbf{J}_a$ denote the Jacobian and augmented Jacobian, respectively. Detailed expressions for calculation of $\mathbf{J}$ are given in reference [15]. Comparable expressions for calculation of the remaining terms of $\mathbf{J}_a$ are easily discerned. Performing QR decomposition on the transpose of $\mathbf{J}_a$ yields the following relationships:

$$\mathbf{J}_a^{\mathrm{T}} = \mathbf{QR} \Rightarrow \mathbf{J}_a = \mathbf{R}^{\mathrm{T}}\mathbf{Q}^{\mathrm{T}}, \qquad \mathbf{Q}^{\mathrm{T}}\mathbf{Q} = \mathbf{I}, \qquad \mathbf{R} = \begin{bmatrix} \mathbf{R}_u \\ \mathbf{0} \end{bmatrix}, \qquad \mathbf{Q} = [\mathbf{Q}_1 \cdots \mathbf{Q}_{N+1}], \tag{7a–c}$$

where $\mathbf{R}_u$ is an $N \times N$ upper diagonal matrix and $\mathbf{Q}$ is an $(N+1) \times (N+1)$ matrix with orthonormal columns.

Note that equation (6) constitutes an under-determined algebraic expression with only one unconstrained degree-of-freedom. For the convergence task, one imposes the additional constraint that the iteration vector $\boldsymbol{\Delta}$ must be normal to the solution curve. Alternatively, for continuation, $\boldsymbol{\Delta}$ should be tangent to the solution curve. On the solution curve, equation (6) reduces to

$$\mathbf{J}_a\mathbf{V} = \mathbf{0}, \tag{8}$$

where $\mathbf{V}$ is tangent to the curve. From equations (7) and (8) it follows that $\mathbf{V} = \mathbf{Q}_{n+1}$. Hence, the QR decomposition directly yields the orthonormal tangent necessary for the continuation task of the iterative method. To converge to the curve, it follows from equations (6–8) that

$$\mathbf{R}^{\mathrm{T}}\boldsymbol{\Phi} + \mathbf{D} = \mathbf{0}, \qquad \boldsymbol{\Phi} \equiv \mathbf{Q}^{\mathrm{T}}\boldsymbol{\Delta} \equiv \begin{bmatrix} \boldsymbol{\Phi}_1 \\ \vdots \\ \boldsymbol{\Phi}_{N+1} \end{bmatrix} \Rightarrow \mathbf{R}_u^{\mathrm{T}} \begin{bmatrix} \boldsymbol{\Phi}_1 \\ \vdots \\ \boldsymbol{\Phi}_N \end{bmatrix} + \mathbf{D} = \mathbf{0}. \tag{9a}$$

Now

$$\boldsymbol{\Delta} = \mathbf{Q}^{\mathrm{T}^{-1}}\boldsymbol{\Phi} = \mathbf{Q}\boldsymbol{\Phi} = [\mathbf{Q}_1 \quad \cdots \quad \mathbf{Q}_N] \begin{bmatrix} \boldsymbol{\Phi}_1 \\ \vdots \\ \boldsymbol{\Phi}_N \end{bmatrix} + \boldsymbol{\Phi}_{N_{+1}}\mathbf{Q}_{N_{+1}}. \tag{9b}$$

But $\mathbf{Q}_{N+1} = \mathbf{V}$ and as one would like $\boldsymbol{\Delta}$ to be normal to $\mathbf{V}$, so one sets $\Phi_{N+1} = 0$. Thus, the solution process involves two steps. First $\boldsymbol{\Phi}$ is calculated from equation (9a) via back substitution. Then $\boldsymbol{\Delta}$ is obtained from equation (9b) via back substitution, as well.

3.3. MODIFICATION OF THE STRATEGY VIA ORDER REDUCTION

Application of the method discussed to a system with many degrees-of-freedom would be computationally prohibitive. Thus, a modified approach is proposed. Consider again the two sections of Figure 2 which are connected by force and displacement vectors. Section (B) can be analyzed completely in the frequency domain using linear algebraic methods. Motion at the connection point to Section (A) can be described by an $N_y \leqslant N_w$-degree-of-freedom vector $\mathbf{y}(\tau)$, which is a linear mapping of $\mathbf{w}(\tau)$ given by

$$\mathbf{y}(\tau) = \mathbf{H}\mathbf{w}(\tau), \qquad \mathbf{y} \equiv [y_1, y_2, \ldots, y_{N_y}]^{\mathrm{T}}, \; \mathbf{H} \equiv \begin{bmatrix} H_{11} & \cdots & H_{1N_w} \\ \vdots & \ddots & \vdots \\ H_{N_y1} & \cdots & H_{N_yN_w} \end{bmatrix}. \tag{10}$$

Likewise, the force vector at this connection point can be described by a vector $\mathbf{F}_y(\tau) \equiv [F_{y1}, F_{y2}, \ldots, F_{yN_y}]^{\mathrm{T}}$ of N_y-degrees-of-freedom. Hence, for Section (B), the frequency-dependent transfer function between $\mathbf{F}_y(\tau)$ and $\mathbf{y}(\tau)$ is easily obtained:

$$\tilde{\mathbf{T}}_{\mathbf{y}}(\omega') \equiv \begin{bmatrix} \tilde{T}_y^{1,1}(\omega') & \cdots & \tilde{T}_y^{1,N_y}(\omega') \\ \vdots & \ddots & \vdots \\ \tilde{T}_y^{N_y,1}(\omega') & \cdots & \tilde{T}_y^{N_y,N_y}(\omega') \end{bmatrix} = \frac{\tilde{\mathbf{y}}}{\tilde{\mathbf{F}}_{\mathbf{y}}}(\omega'), \qquad \tilde{T}_y^{r,s}(\omega') = \frac{\tilde{y}_r}{\tilde{F}_{y_s}}(\omega'). \tag{11}$$

Here, superscript ˜ denotes a complex number and ω' is an arbitrary response frequency. Now, the mnth approximate solution to the problem is modified by replacing equations (3b), (4b) (5) and (6) with the following:

$$\mathbf{y}^{mn}(\tau) = \mathbf{a}_0^y + \sum_{k=1}^{mn} \mathbf{a}_{2k-1}^y \sin(k\tau) + \mathbf{a}_{2k}^y \cos(k\tau), \tag{12a}$$

where

$$\mathbf{a}_k^y \equiv [a_k^{y_1}, a_k^{y_2}, \ldots, a_k^{yN_y}]^{\mathrm{T}}, \qquad \boldsymbol{\alpha}^y \equiv [\mathbf{a}_0^y \, \mathbf{a}_1^y \cdots \mathbf{a}_{4mn}^y],$$

$$D_0^{ymn}(\boldsymbol{\alpha}) \equiv \sum_{s=1}^{N_y} \{\mathrm{Re}[\tilde{T}_y^{r,s}(0)] a_0^{F_{ys}}\} - a_0^{yr} = 0, \tag{12b}$$

$$D_{2k-1}^{ymn}(\boldsymbol{\alpha}) \equiv \sum_{s=1}^{N_y} \left\{ \mathrm{Re}\left[\tilde{T}_y^{r,s}\left(\frac{k\omega}{m}\right)\right] a_{2k-1}^{F_{ys}} + \mathrm{Im}\left[\tilde{T}_y^{r,s}\left(\frac{k\omega}{m}\right)\right] a_{2k}^{F_{ys}} \right\} - a_{2k-1}^{yr} = 0, \tag{12c}$$

$$D_{2k}^{ymn}(\boldsymbol{\alpha}) \equiv \sum_{s=1}^{N_y} \left\{ \mathrm{Re}\left[\tilde{T}_y^{r,s}\left(\frac{k\omega}{m}\right)\right] a_{2k}^{F_{ys}} - \mathrm{Im}\left[\tilde{T}_y^{r,s}\left(\frac{k\omega}{m}\right)\right] a_{2k-1}^{F_{ys}} \right\} - a_{2k}^{yr} = 0, \tag{12d}$$

where

$$\boldsymbol{\alpha} \equiv [\boldsymbol{\alpha}^x \, \boldsymbol{\alpha}^y]^{\mathrm{T}}, \qquad r = 1, \ldots, N_y, \qquad k = 1, \ldots, 2mn$$

and

$$a_j^{F_{ys}} \equiv \mathscr{F}_j[\mathrm{F}_{y_s}^{mn}(\tau)], \qquad j = 0, \ldots, 4mn.$$

Also,

$$R = \sum_{j=0}^{4nm} \left\{ \sum_{s=1}^{N_x} \left| D_j^{x^{mn}} \right|^2 + \sum_{s=1}^{N_y} \left| D_j^{y^{mn}} \right|^2 \right\},$$

$$\mathbf{D}^y \equiv [\mathbf{D}_0^{y^{mn}} \cdots \mathbf{D}_{4nm}^{y^{mn}}]^{\mathrm{T}},$$

$$\mathbf{J}_a \equiv \left[\mathbf{J} \frac{\partial \mathbf{D}}{\partial \Omega} \right] \equiv \begin{bmatrix} \dfrac{\partial \mathbf{D}^x}{\partial \boldsymbol{\alpha}^x} & \dfrac{\partial \mathbf{D}^x}{\partial \boldsymbol{\alpha}^y} & \dfrac{\partial \mathbf{D}^x}{\partial \Omega} \\ \dfrac{\partial \mathbf{D}^y}{\partial \boldsymbol{\alpha}^x} & \dfrac{\partial \mathbf{D}^y}{\partial \boldsymbol{\alpha}^y} & \dfrac{\partial \mathbf{D}^y}{\partial \Omega} \end{bmatrix}. \tag{12e}$$

Thus, the number of coupled non-linear equations to be iteratively solved remains fixed at $N = (N_x + N_y) \times (4nm + 1)$ regardless of the number of degrees-of-freedom N_w in Section (B). Once the non-linear solution is obtained, the response of any degree-of-freedom in Section (B) is quickly found via linear algebraic techniques.

It should be mentioned that the form of reduction outlined above does not imply the higher modes or degrees-of-freedom have been removed from the problem formulation. Hence, inaccuracies that may result from other methods that specifically truncate higher vibration modes are not an issue here. Also, it is intuitively argued that the convergence properties of the conventional Galerkin method should be applicable to this modified strategy since essentially the same "weak" form solution of the governing differential equations is still being sought. A more rigorous analysis is left for a future article.

A block diagram outlining the entire method is provided in Figure 3. Typical expressions for calculation of the modified terms in $\mathbf{J}_a$ are provided for the first example case in Section 4.

4. METHOD VALIDATION VIA DIGITAL AND ANALOG SIMULATION STUDIES

4.1. EXAMPLE CASE I

In order to first verify the proposed non-linear solution strategy and demonstrate its capabilities, two physical systems, fitting the framework of Figures 1 and 2, are considered.

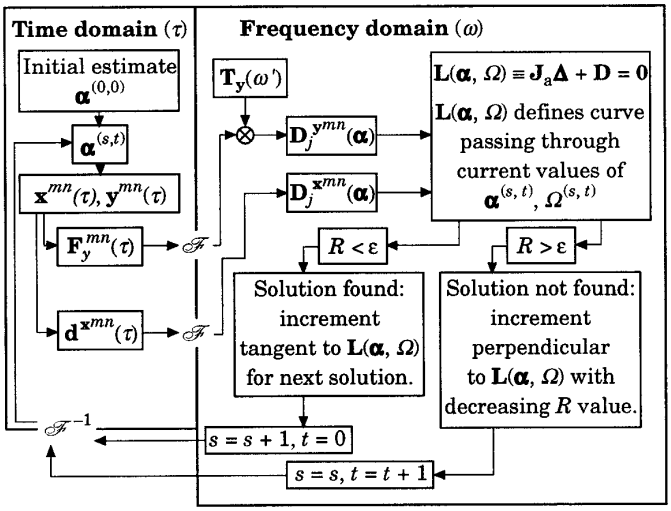

Figure 3. The enhanced Galerkin method.

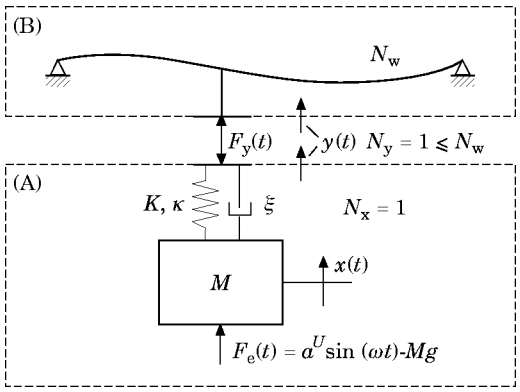

Figure 4. Example Case I: rigid body connected to a simply supported beam through a non-linear spring.

Predictions based on the proposed strategy are compared to solutions obtained via digital (direct time) integration and, for the first system, analog computer simulation. The first example case system, a mass connected to a simply supported beam through a non-linear stiffness element, is chosen to highlight how order reduction is employed to greatly reduce the complexity of the problem. Also, excitation conditions are selected which result in a response containing sub and superharmonic components. An automotive hydraulic engine mounting system is considered as the second example case in Section 5. The mount model, based on prior experimental analyses of actual hydraulic mounts [21–23], possesses non-linearities defined in both the time and frequency domain.

The system of Figure 4 is subjected to harmonic excitation in the vertical direction. The simply supported beam contains the key ingredients found in many components of assembled structures. It is spatially extended with multiple degrees-of-freedom and behaves in a linear fashion for small amplitude vibration. For this system one has $N_x = 1$ and $N_w =$ the number of degrees-of-freedom considered in the beam. Note that either a distributed modal or lumped mass model could be used for the beam. In this study a modal strategy is employed.

For the simply supported beam, the dynamics can be described by Euler's equation [24]:

$$\rho A\ddot{u}(s, t) + EI\frac{\partial^4 u}{\partial s^4}(s, t) = F_y(t)\delta(s - s_b). \tag{13}$$

Here, ρ, A, E, I, δ, and s_b refer to the beam material density, beam cross sectional area, Young's modulus of the beam, beam moment of inertia, the Dirac delta function, and the axial position of the nonlinear element connection to the beam, respectively. (Also refer to Appendix A.2.) Modal decomposition is performed to obtain N_w coupled, ordinary differential equations. At an arbitrary frequency ω' one has

$$F_y(t) = \tilde{F}_y e^{i\omega' t}, \qquad u(s, t) = \sum_{j=1}^{N_w} \tilde{u}_j \sin(j\pi s/l_s)\, e^{i\omega' t}, \tag{14a,b}$$

which yields

$$m_b \mathbf{\Psi}^{-1}(\omega')\begin{bmatrix} \tilde{u}_1 \\ \vdots \\ \tilde{u}_{N_w} \end{bmatrix} = \mathbf{H}^T \tilde{F}_y, \qquad \mathbf{\Psi} \equiv \begin{bmatrix} \tilde{\Psi}_1 & \cdots & 0 \\ \vdots & \ddots & \vdots \\ 0 & \cdots & \tilde{\Psi}_{N_w} \end{bmatrix},$$

with

$$\tilde{\Psi}_j \equiv 1(\omega_j^2 - \omega^2 + i2\zeta_j\omega\omega_j), \qquad \mathbf{H} \equiv [\sin(\pi s_b/l_s) \cdots \sin(N_w \pi s_b/l_s)],$$
$$\omega_j \equiv \sqrt{EI/\rho A}\,(j\pi/l_s)^2, \qquad m_b \equiv \rho A l_s/2, \qquad j = 1, \ldots, N_w. \tag{15}$$

Here, l_s refers to the length of the beam. Note that proportional modal damping ζ_j has been assumed. From equations (14) and (15), it follows that

$$\tilde{y} = \mathbf{H}[\tilde{u}_1 \cdots \tilde{u}_{N_b}]^{\mathrm{T}}, \qquad \tilde{T}_y(\omega') \equiv (\tilde{y}/\tilde{F}_y)(\omega') = (1/m_b)\mathbf{H}\boldsymbol{\Psi}(\omega')\mathbf{H}^{\mathrm{T}}. \tag{16a,b}$$

Here, note that $N_y = 1$ regardless of N_w, the number of beam modes considered.

For Section (A), equation (2a) reduces to the scalar expression

$$\mathrm{d}^x(\tau) \equiv (m/\omega)^2(1/M)[a^U \sin(m\tau) - Mg - F_y(\tau)] - \ddot{x}(\tau) = 0. \tag{17}$$

The junction force $F_y(\tau)$ is described by

$$F_y(\tau) = K[1 + \kappa(x(\tau) - y(\tau))^2](x(\tau) - y(\tau)) + (\dot{x}(\tau) - \dot{y}(\tau))2\xi\sqrt{MK}(\omega/m)). \tag{18}$$

Based on the above formulation, the resulting determining equations for the Galerkin procedure can be expressed as

$$D_j^{x^{mn}}(\boldsymbol{\alpha}) \equiv \mathscr{F}_j[\mathrm{d}^x(\tau)] = 0, \quad j = 0, \ldots, 4nm, \quad D_0^{y^{mn}} mn0(\alpha) = \mathrm{Re}[\tilde{T}_y(0)]a_0^{F_y} - a_0^y = 0, \tag{19a,b}$$

$$D_{2k-1}^{y^{mn}}(\alpha) = \mathrm{Re}[\tilde{T}_y(k\omega/m)]a_{2k-1}^{F_y} + \mathrm{Im}[\tilde{T}_y(k\omega/m)]a_{2k}^{F_y} - a_{2k-1}^y = 0,$$
$$k = 1, \ldots, 2mn, \tag{19c}$$

$$D_{2k}^{y^{mn}}(\boldsymbol{\alpha}) = \mathrm{Re}[\tilde{T}_y(k\omega/m)]a_{2k}^{F_y} - \mathrm{Im}[\tilde{T}_y(k\omega/m)]a_{2k-1}^{F_y} - a_{2k}^y = 0, \qquad k = 1, \ldots, 2mn. \tag{19d}$$

Detailed expressions for calculation of the elements of the augmented Jacobian matrix based on the conventional Galerkin method, $\partial D_j^{x^{mn}}/\partial\alpha$ and $\partial D_j^{x^{mn}}/\partial\Omega$, $j = 0, \ldots, 4mn$, can be derived from reference [15]. Equations for calculation of other elements of $\mathbf{J_a}$ are as follows, for $q = x$ or y:

$$\frac{\partial D_0^{y^{mn}}}{\partial a_j^q}(\boldsymbol{\alpha}) = \mathrm{Re}[\tilde{T}_y(0)]\mathscr{F}_0\left[\frac{\partial F_y^{mn}(\tau)}{\partial q}\frac{\partial q}{\partial a_j^q} + \frac{\partial F_y^{mn}(\tau)}{\partial \dot{q}}\frac{\partial \dot{q}}{\partial a_j^q}\right] - \delta_{qy}\delta_{j0}, \qquad j = 0, \ldots, 4mn, \tag{20a}$$

$$\frac{\partial D_{2k-1}^{y^{mn}}}{\partial a_j^q}(\boldsymbol{\alpha}) = \mathrm{Re}\left[\tilde{T}_y\left(\frac{k\omega}{m}\right)\right]\mathscr{F}_{2k-1}\left[\frac{\partial F_y^{mn}(\tau)}{\partial q}\frac{\partial q}{\partial a_j^q} + \frac{\partial F_y^{mn}(\tau)}{\partial \dot{q}}\frac{\partial \dot{q}}{\partial a_j^q}\right]$$
$$+ \mathrm{Im}\left[\tilde{T}_y\left(\frac{k\omega}{m}\right)\right]\mathscr{F}_{2k}\left[\frac{\partial F_y^{mn}(\tau)}{\partial q}\frac{\partial q}{\partial a_j^q} + \frac{\partial F_y^{mn}(\tau)}{\partial \dot{q}}\frac{\partial \dot{q}}{\partial a_j^q}\right]$$
$$- \delta_{qy}\delta_{j(2k-1)}, \qquad j = 0, \ldots, 4mn, \qquad k = 1, \ldots, 2mn, \tag{20b}$$

$$\frac{\partial D_{2k}^{y^{mn}}}{\partial a_j^q}(\boldsymbol{\alpha}) = \mathrm{Re}\left[\tilde{T}_y\left(\frac{k\omega}{m}\right)\right]\mathscr{F}_{2k}\left[\frac{\partial F_y^{mn}(\tau)}{\partial q}\frac{\partial q}{\partial a_j^q} + \frac{\partial F_y^{mn}(\tau)}{\partial \dot{q}}\frac{\partial \dot{q}}{\partial a_j^q}\right]$$
$$- \mathrm{Im}\left[\tilde{T}_y\left(\frac{k\omega}{m}\right)\right]\mathscr{F}_{2k-1}\left[\frac{\partial F_y^{mn}(\tau)}{\partial q}\frac{\partial q}{\partial a_j^q} + \frac{\partial F_y^{mn}(\tau)}{\partial \dot{q}}\frac{\partial \dot{q}}{\partial a_j^q}\right] \tag{20c}$$
$$- \delta_{gy}\delta_{j(2k)}, \quad j = 0, \ldots, 4mn, \qquad k = 1, \ldots, 2mn,$$

$$\frac{\partial D_0^{ymn}}{\partial \Omega}(\boldsymbol{\alpha}) = \mathrm{Re}[\tilde{T}_y(0)]\mathscr{F}_0\left[\frac{\partial F_y^{mn}(\tau)}{\partial \Omega}\right] + \mathrm{Re}\left[\frac{\partial \tilde{T}_y}{\partial \Omega}(0)\right]a_0^{F_y}, \tag{20d}$$

$$\frac{\partial D_{2k-1}^{ymn}}{\partial \Omega}(\boldsymbol{\alpha}) = \mathrm{Re}\left[\tilde{T}_y\left(\frac{k\omega}{m}\right)\right]\mathscr{F}_{2k-1}\left[\frac{\partial F_y^{mn}(\tau)}{\partial \Omega}\right] + \mathrm{Im}\left(\tilde{T}_y\left(\frac{k\omega}{m}\right)\right]\mathscr{F}_{2k}\left[\frac{\partial F_y^{mn}(\tau)}{\partial \Omega}\right]$$
$$+ \mathrm{Re}\left[\frac{\partial \tilde{T}_y}{\partial \Omega}\left(\frac{k\omega}{m}\right)\right]a_{2k-1}^{F_y} + \mathrm{Im}\left[\frac{\partial \tilde{T}_y}{\partial \Omega}\left(\frac{k\omega}{m}\right)\right]a_{2k}^{F_y}, \qquad k = 1, \ldots, 2mn, \tag{20e}$$

$$\frac{\partial D_{2k}^{ymn}}{\partial \Omega}(\boldsymbol{\alpha}) = \mathrm{Re}\left[\tilde{T}_y\left(\frac{k\omega}{m}\right)\right]\mathscr{F}_{2k}\left[\frac{\partial F_y^{mn}(\tau)}{\partial \Omega}\right] - \mathrm{Im}\left(\tilde{T}_y\left(\frac{k\omega}{m}\right)\right]\mathscr{F}_{2k-1}\left[\frac{\partial F_y^{mn}(\tau)}{\partial \Omega}\right]$$
$$+ \mathrm{Re}\left[\frac{\partial \tilde{T}_y}{\partial \Omega}\left(\frac{k\omega}{m}\right)\right]a_{2k}^{F_y} - \mathrm{Im}\left[\frac{\partial \tilde{T}_y}{\partial \Omega}\left(\frac{k\omega}{m}\right)\right]a_{2k-1}^{F_y}, \quad k = 1, \ldots, 2mn, \tag{20f}$$

Thus, the number of coupled non-linear algebraic equations to be iteratively solved remains fixed at $N = 2 \times (4nm + 1)$ regardless of the number of degrees-of-freedom used to model the simply supported beam. For this study, the analytical solution for a simply supported beam was used to calculate the distributive modal degrees-of-freedom of the base. For a complex structure where closed form analysis solutions may not be available, discrete models obtained by other means such as finite element analysis, experimental modal analysis or driving point mobility measurements could be used instead to calculate $\tilde{\mathbf{T}}_y(\omega')$.

4.2. DIGITAL SIMULATION OF CASE I

For the case of $N_w = 1$, the resulting two-degree-of-freedom non-linear system is simulated using *MATLAB Simulink* software [25] with a Runga-Kutta 4/5 predictor/corrector integration routine. Steady state solutions for harmonic excitation are found and compared to solutions yielded by the "enhanced" Galerkin method. Example case parameter and excitation values are provided in Table 1. Note that for this run a zero static load ($g = 0$) is used. Results of the study are shown in Figures 5 and 6. In Figure 5, a main solution path and a secondary closed loop solution path are shown. On the main path, odd order superharmonics are present as the system goes through a strong stiffness hardening resonance. Of course, numerical integration is unable to track the unstable portion of the solution curve predicted by the Galerkin approach. On the secondary closed loop, sub- and ultra-subharmonics of the odd one third order (1/3, 3/3, 5/3, . . .) are present. Only a small section of this curve is stable. In Figure 6, two significantly different stable solutions are shown in the time domain for identical excitation conditions, serving as further testimony to the degree of non-linearity in the system considered. In both Figures 5 and 6, the enhanced Galerkin method results match numerical simulation results excellently for both sub and superharmonic responses.

4.3. ANALOG COMPUTER SIMULATION OF CASE I

A Comdyna GP-6 analog computer was used to simulate the non-linear system. The analog computer, while still providing greater control over the nature of the governing equations, introduces some issues that one must consider in an experimental study. For example, there is greater uncertainty in actual system parameter values, and additionally, system outputs are measured as voltages via instrumentation in the same way that experimental outputs from various sensors are measured. Signal to noise ratio,

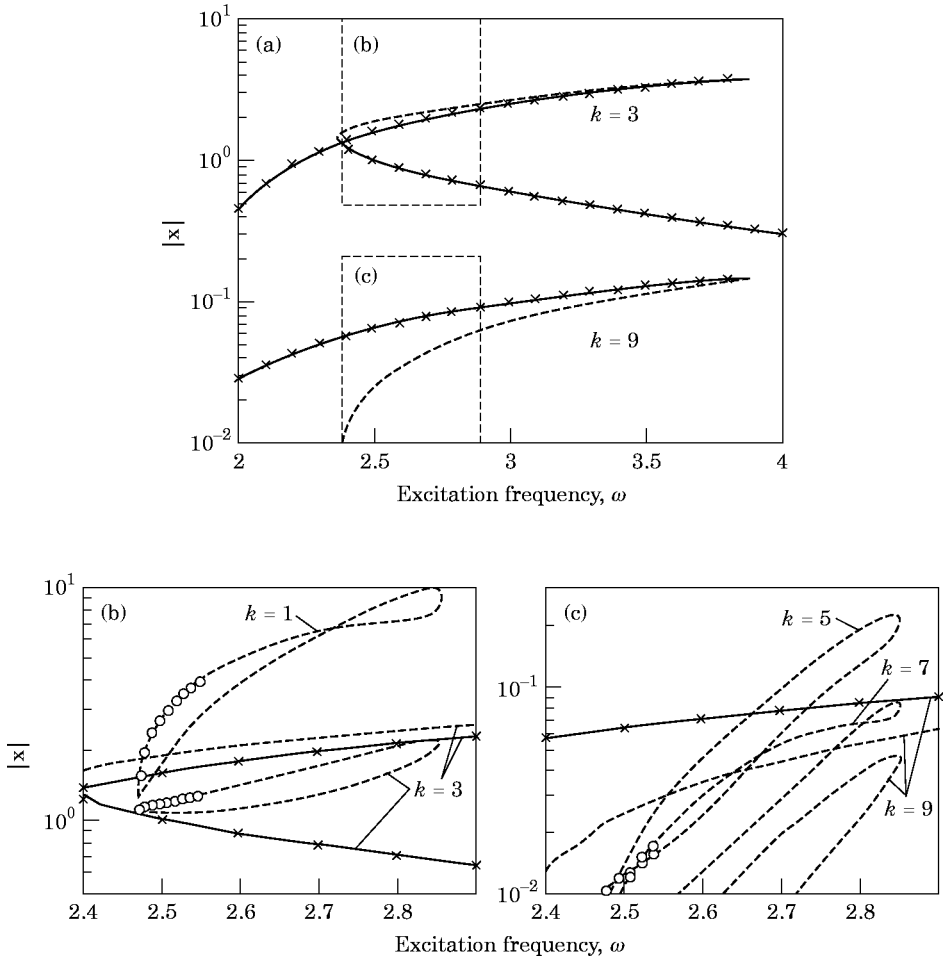

Figure 5. System response for digital computer study of example Case I. Selected super and subharmonic response of rigid mass motion x. Here $m = 3$ and $n = 15$. Hence, the curve denoted by k is the $k/3$rd harmonic. Key: ——, enhanced Galerkin method (– – – unstable); x x x o o o, direct time integration. (a): Main solution path. (b) Close-up showing main and (c) secondary closed-loop solution paths.

saturation, and amplitude and time scaling are key concerns. A schematic of the analog computer setup is shown in Figure 7. In this case, response of $\ddot{y}$ to swept harmonic excitation was recorded via the order tracking function available on the Hewlett Packard 35670 Dynamic Signal Analyzer. Sine frequency was swept slowly for both increasing and decreasing values. Typically, the system response converges asymptotically to its steady state response under harmonic excitation, if the sweep rate is sufficiently slow. Studies at

TABLE 1

Parameter values for example Case I *Figure* 4

Digital simulation			Analog simulation		
$a^U = 4{\cdot}8$	$m_b = 1$	$\kappa = 0{\cdot}1$	$a^U = 1{\cdot}27$	$m_b = 0{\cdot}586$	$\kappa = -0{\cdot}8477$
$g = 0$	$N_w = 1$	$\omega_1 = \sqrt{2}$	$g = 9{\cdot}8$	$N_w = 1$	$\omega_1 = 3{\cdot}29$
$K = 1$	$\zeta_1 = 0{\cdot}025/\sqrt{2}$	$\xi = 0{\cdot}025$	$K = 65$	$\zeta_1 = 0{\cdot}042$	$\xi = 0{\cdot}005$
$M = 1$	$s_b/l_s = 1/2$		$M = 2{\cdot}64$	$s_b/l_s = 1/2$	

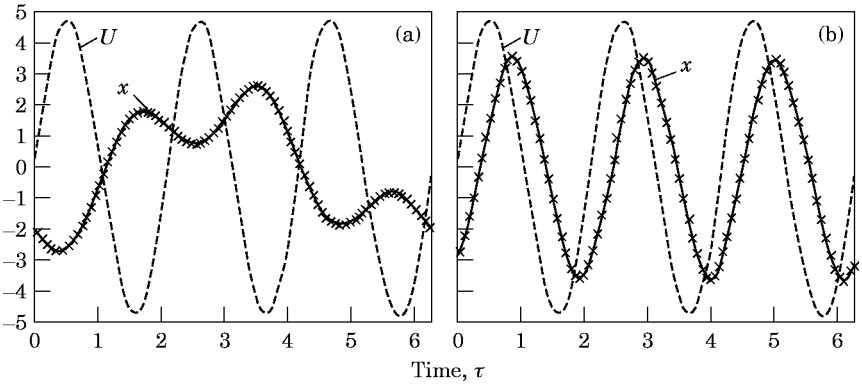

Figure 6. Time response of example Case I at $\omega = 2{\cdot}48$. Key: ——, direct time integration of x; X X X, enhanced Galerkin Method of x; — — —, excitation force $a^U \sin(\tau)$. (a) Closed loop path stable solution. (b) Main path, large amplitude stable solution.

other rates confirmed that asymptotic convergence within instrumentation precision had been reached.

Different parameter values from the digital simulation run, which are provided in Table 1, were used for this run. Results are shown in Figure 8 for the resonance associated with out-of-phase motion between the beam and rigid mass. The first three integer harmonics were the only components of the response above the instrumentation noise floor. Note that multi-valued frequency response curves were obtained via analog computer. While a primary path with a softening resonance was computed, no secondary loops were found for this set of parameter values. Again, the enhanced Galerkin method agrees very well with simulation results, given the modeling uncertainties involved in the analog computer implementation [3]. Even integer harmonics occur in this case because of the asymmetry in stiffness caused by a finite static load.

5. PRACTICAL EXAMPLE: HYDRAULIC ENGINE MOUNT SYSTEM

5.1. EXAMPLE CASE II

Consider the automotive hydraulic engine mounting system of Figure 9. This system and the accompanying model are based on several papers by Kim and Singh [21–23] covering

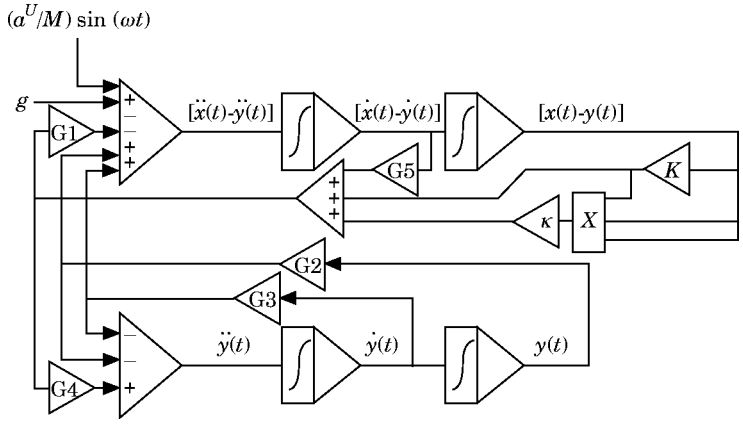

Figure 7. Diagram for analog computer simulation of Case I. See Table I for parameter values. Here $G1 = (1/M) + (1/m_b)$, $G2 = \omega_1^2$, $G3 = 2\zeta_1\omega_1$, $G4 = 1/m_b$, and $G5 = 2\xi\sqrt{MK}$.

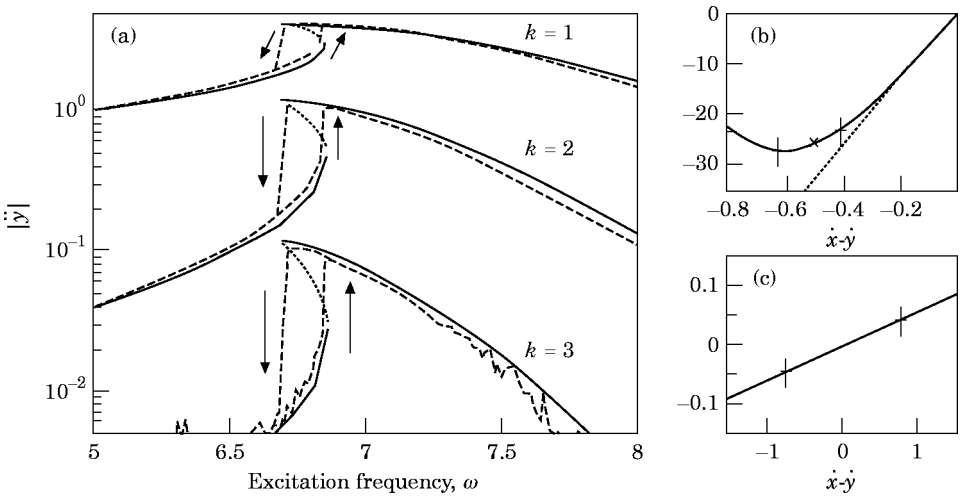

Figure 8. System response for analog computer study of excample Case I. (a) Selected superharmonic responses of the junction point vertical acceleration $\ddot{\mathbf{y}}$. Here $m = 1$ and $n = 5$. Hence, the curve denoted by k is the kth harmonic. Key: ——, enhanced Galerkin method (– – –, unstable), — — —, analog computer. (b) Mount elastic force. Key: – – – –, linear force; ——, cubic + linear force; x, static deflection. (c) Mount dissipative force. Key: ——, viscous damping force. In parts (b) and (c), | | denotes the operation range at $\omega = 6{\cdot}75$ (large amplitude solution).

theoretical and experimental studies of hydraulic mounts employing an inertia track between two fluid chambers. The inertia track may act as an "absorber" tuned to the fundamental engine mounting resonance and it provides inertia-augmented damping. Only vertical translational motion is considered. The engine is driven by a harmonic vertical excitation force of frequency ω, representing imbalance forces associated with engine operation. The engine is assumed to be a rigid body of mass M_e and the chassis is modeled as a single-degree-of-freedom linear spring mass-damper. System response is assumed to be periodic with superharmonic content up to the nth order and subharmonic content up

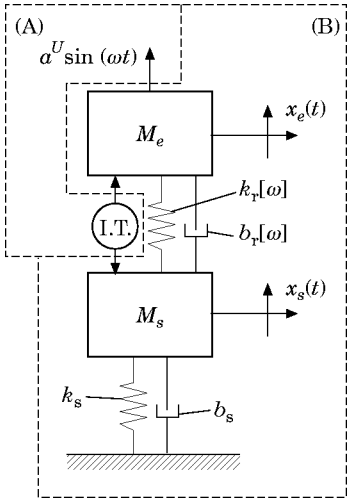

Figure 9. Example Case II: hydraulic engine mounting system. Here, I. T. refers to the inertia track, and subscripts e, r and s refer to parameters associated with the engine, rubber part of the engine mount and the automotive chassis, respectively.

to the mth order. Equations are written as functions of a non-dimensional time variable $\tau = \omega t/m$.

The hydraulic mount consists of a stiffness and damping element in parallel with a single-degree-of-freedom resonator. As in the references [21–23], system equations are defined around a static equilibrium point; hence, the static (gravitational) force is not present in the following formulation. The stiffness and damping elements, which account for the rubber portion of the mount, are non-linear and are explicitly defined in the frequency domain. A polynomial expression in the frequency domain can be used to approximate them. Consequently, for the engine (e) and mount rubber (r) one has:

$$(\omega^2/m^2)M_e\ddot{x}_e(\tau) + (\omega/m)b_r[\omega][\dot{x}_e(\tau) - \dot{x}_s(\tau)] + k_r[\omega][x_e(\tau) - x_s(\tau)] = F_U(\tau), \quad (21a)$$

$$F_U(\tau) = A_p[p_1(\ \tau) - \bar{p}] + a^U \sin(m\tau). \quad (21b)$$

Refer to Appendix A.3 for symbol identification. For the chassis (s) degree-of-freedom one has

$$(\omega^2/m^2)M_s\ddot{x}_s(\tau) + (\omega/m)b_s\ddot{x}_s(\tau) + k_s x_s(\tau) = F_L(\tau) + k_r[\omega][x_e(\tau) - x_s(\tau)] + (\omega/m)b_r[\omega][\dot{x}_e(\tau) - \dot{x}_s(\tau)], \quad (22a)$$

$$F_L(\tau) = -A_p[p_1(\tau) - \bar{p}] \quad (22b)$$

The single-degree-of-freedom non-linear resonator, accounting for dynamics associated with the upper and lower fluid chambers and the inertia track connecting them, can be explicitly defined in the time domain by a lumped parameter model [21]:

$$(m^2/\omega^2 I)[p_2(\tau) - p_1(\tau)] - (\lambda/I)\dot{v}(\tau)^2 \operatorname{sign}[\dot{v}(\tau)] - \ddot{v}(\tau) = 0, \quad (23a)$$

with

$$p_2(\tau) = 5{\cdot}26 \times 10^{-3} V_2(\tau)^{2{\cdot}5} - 8{\cdot}9 \times 10^{-8} V_2(\tau)^6 + 1{\cdot}41 \times 10^{-8} V_2(\tau)^{6{\cdot}5} + p_{atm}, \quad (23b)$$

$$p_1(\tau) = \begin{cases} -6{\cdot}4V_1(\tau) + 29{\cdot}2V_1(\tau)^{7/6} + p_{atm}, & V_1(\tau) \geqslant 0, \\ p_{atm}\bar{V}_{air}/(\bar{V}_{air} + |V_1(\tau)|), & V_1(\tau) < 0, \end{cases} \quad (23c)$$

$$V_1(\tau) = \bar{V}_1 + v(\tau) - A_p[x_e(\tau) - x_s(\tau)], \qquad V_2(\tau) = \bar{V}_2 - v(\tau), \qquad I = \rho_g l/A. \quad (23d\text{–}f)$$

Thus, one has a three-degree-of-freedom model for the overall sytem. A solution for the linear chassis degree-of-freedom and non-linear engine/rubber degree-of-freedom, defined in the frequency domain, can be explicitly written algebraically in the frequency domain. Consider harmonic excitation of frequency ω'. Then, one has an harmonic displacement and force response at the connection points to the non-linear hydraulic degree-of-freedom of the following form:

$$x_e(\tau) = \tilde{x}_e\, e^{i\omega'\tau}, \qquad x_s(\tau) = \tilde{x}_s\, e^{i\omega'\tau}, \qquad F_U(\tau) = \tilde{F}_U\, e^{i\omega'\tau}, \qquad F_L(\tau) = \tilde{F}_L\, e^{i\omega'\tau}. \quad (24a\text{–}d)$$

Consequently, a transfer function in the frequency domain between displacement and force at the connection points to Section (A) can be written as such:

$$\tilde{\mathbf{T}}(\omega') \equiv \begin{bmatrix} \dfrac{\tilde{x}_e}{\tilde{F}_U} & \dfrac{\tilde{x}_e}{\tilde{F}_L} \\ \dfrac{\tilde{x}_s}{\tilde{F}_U} & \dfrac{\tilde{x}_e}{\tilde{F}_L} \end{bmatrix} = \begin{bmatrix} k_r(\omega') - \omega^2 m_e + i\omega b_r(\omega') & -k_r(\omega') - i\omega' b_r(\omega') \\ -k_r(\omega') - i\omega b_r(\omega') & k_r(\omega') + k_s - \omega^2 m_s + i\omega'[b_r(\omega') + b_s] \end{bmatrix}. \quad (25)$$

TABLE 2

Parameter values for example case II *of figure* 9

Digital simulation		
$A = 0{\cdot}2726\ \text{cm}^2$	$\lambda = 1{\cdot}1 \times 10^{-3}\ \text{kPa s}^2/\text{cm}^3$	$\rho_g = 1{\cdot}059 \times 10^{-3}\ \text{kg/cm}^3$
$A_p = 5{\cdot}027 \times 10^{-3}\ \text{m}^2$	$M_e = 122{\cdot}7\ \text{kg}$	$\bar{V}_1 = 0{\cdot}715\ \text{cm}^3$
$a^U = 100\ \text{N}$	$M_s = 270\ \text{kg}$	$\bar{V}_2 = 28{\cdot}251\ \text{cm}^3$
$b_s = 1400\ \text{Ns/m}$	$m = 1, n = 15$	$\bar{V}_{air} = 4\ \text{cm}^3$
$k_s = 2 \times 10^4\ \text{N/m}$	$\bar{p} = 116{\cdot}4\ \text{kPa}$	$\omega/2\pi = 3\text{–}20\ \text{Hz}$
$l = 2{\cdot}5\ \text{cm}$	$p_{atm} = 101{\cdot}232\ \text{kPa}$	

Hence, in this example case, three-degrees-of-freedom still remain for solution by the enhanced Galerkin method. This is because there were as many force/motion pairs connecting Section (A) to Section (B) as there were degrees of-freedom in Section (B); $\mathbf{y} \equiv [x_e\ x_s]^T$, $\mathbf{F}_\mathbf{y} \equiv [F_U\ F_L]^\mathrm{T}$, $N_y = 2$. However, this approach easily accomodates two complexities that could not be handled by the conventional Galerkin method or by the direct time integration technique. First, additional linear degrees-of-freedom or frequency-defined non-linear degrees-of-freedom could be used to model the chassis or mount, $N_w > 2$, without an increase in order of the iterative method, as long as additional connections to Section (A) are not added. Second, this approach has enabled use of an exact expression for the frequency dependent stiffness and damping values of the mount rubber.

5.2. DIGITAL SIMULATION OF CASE II

The system response is studied over a range of excitation frequencies for three different mount rubber models. System parameter values, provided in Table 2, are selected from references [21–23] and are based on experimental measurements of actual hydraulic engine mounts and systems. Note that the single inertia track path in this study is identical to the path of least resistance in the dual path configuration "A" of reference [21]. A single path configuration was used for the sake of clarity.

Experimental values for mount rubber stiffness k_r and damping b_r as a function of frequency ω' are given graphically in reference [22]. The following polynomial expressions approximate the experimental values:

$$k_r(\omega') = 2{\cdot}7 \times 10^5 + 1{\cdot}47 \times 10^5 \omega'^{-1}(\text{N/m}),$$

$$b_r(\omega') = 478{\cdot}0 + 9{\cdot}29\omega' - 4{\cdot}03 \times 10^{-2}\omega'^2 + 7{\cdot}02 \times 10^{-5}\omega^3(\text{Ns/m}), \qquad (26a,b)$$

In the enhanced Galerkin method, these values are easily incorporated into $\tilde{\mathbf{T}}(\omega')$, where for a given excitation frequency ω, one has $\omega' = q\omega/s$ with $q = 0, \ldots, n$ and $s = 1, \ldots, m$. This model for $k_r[\omega]$ and $b_r[\omega]$ will be referred to as the exact non-linear model. While it is impossible to use it in a direct time integration approach, a quasi-linear model can be substituted, where for a given excitation frequency ω it can be assumed $k_r(q\omega/s) = k_r(\omega)$ and $b_r(q\omega/s) = b_r(\omega)$ for any value of q/s. In other words, for a given ω, k_r and b_r have the same values for all frequencies in the response. Finally, constant values for k_r and b_r could be assumed, i.e. $k_r[\omega] = \bar{k}_r$ and $b_r[\omega] = \bar{b}_r$.

First, the solutions obtained via the enhanced Galerkin method and direct time integration (using *MATLAB SIMULINK* software [25]) are compared in Figures 10 and 11. Response of $\ddot{v}_1$ and $\ddot{x}_s$ to harmonic excitation with the quasi-linear rubber model are shown. Note that the local non-linearity in the inertia track, Section (A), has affected

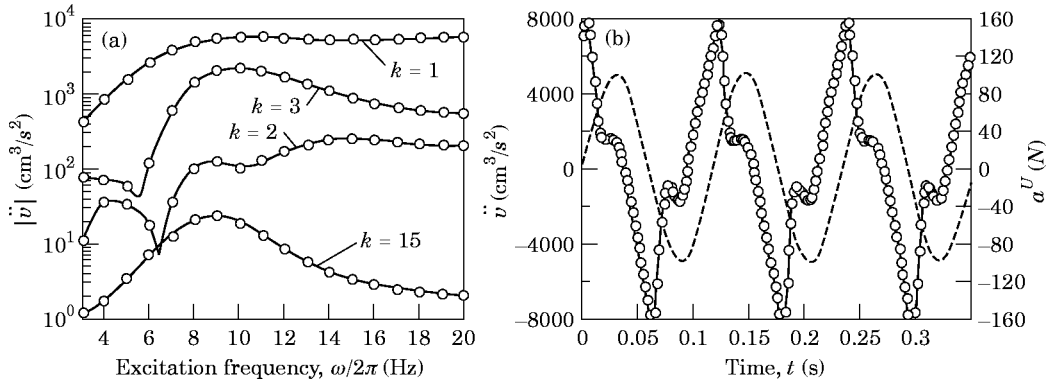

Figure 10. Hydraulic engine mounting system response with quasi-linear mount rubber model. (a) Selected superharmonic responses of inertia work track volume acceleration $\ddot{v}$. Here $m = 1$ and $n = 15$. Hence, the curve denoted by k is the kth harmonic. Key: ——, enhanced Galerkin method; o o o, direct time integration. (b) Time response at $\omega/2\pi = 8{\cdot}5$ Hz of $\ddot{v}$. Key: ——, direct time integration; o o o, enhanced Galerkin method; — — —, excitation force, a^U.

the global system response, as evident in the super and subharmonic content of $\ddot{x}_s$, a variable located in Section (B). The response is compared for the three different mount rubber models in Figure 12. Only minimal differences in the three responses are observed, which suggests that the simplified models may be acceptable in this case.

6. CONCLUSION

An efficient computational methodology has been formulated for the analysis of many degree-of-freedom systems with local non-linearities defined in the time and/or frequency domains. A Galerkin-based computational method has been enhanced with a form of order reduction and numerical continuation. Order reduction enables inclusion of the extensive and necessary, but often linear, assembled component dynamics with minimal computational cost. Additionally, the reduction approach developed in this study allows for non-linearities defined in both the time and frequency domain to be explicitly expressed and efficiently handled simultaneously. A continuation scheme facilitates parametric

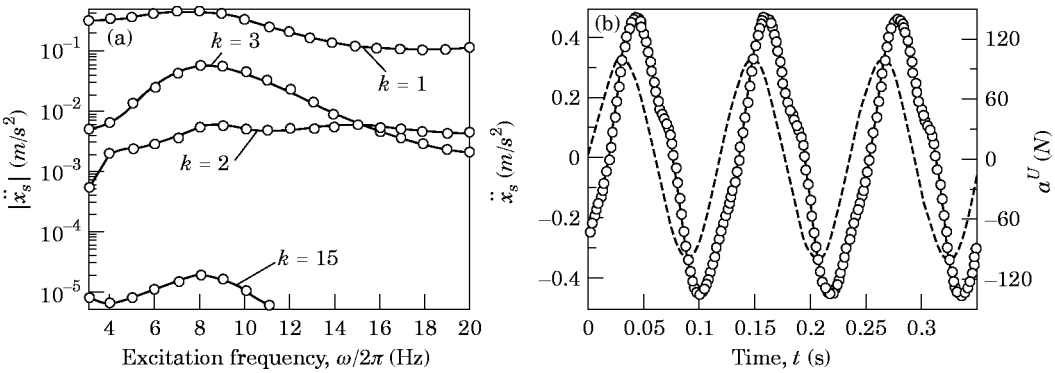

Figure 11. Hydraulic engine mounting system response with quasi-linear mount rubber model. (a) Selected superharmonic responses of chassis acceleration $\ddot{x}_s$. Hence $m = 1$ and $n = 15$. Hence, the curve denoted by k is the kth harmonic. Key: ——, enhanced Galerkin method; o o o, direct time integration. (b) Time response at $\omega/2\pi = 8{\cdot}5$ Hz of $\ddot{x}_s$. Key: ——, direct time integration; o o o, enhanced Galerkin method; — — —, excitation force, a^U.

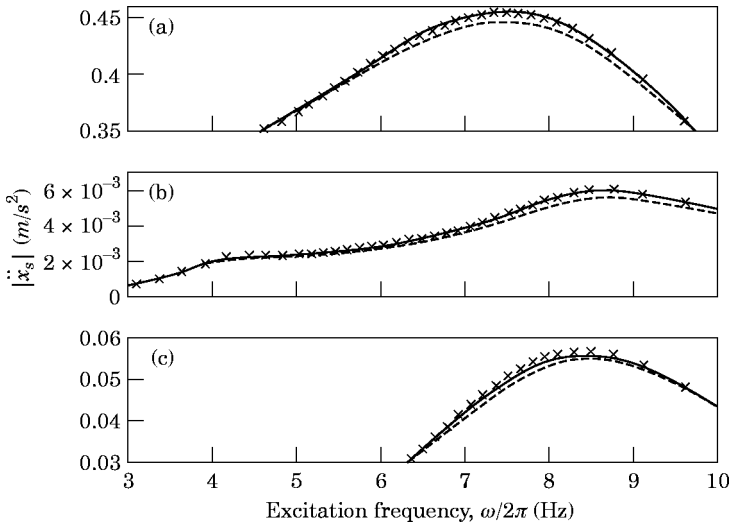

Figure 12. Hydraulic engine mounting system response with different mount rubber models. Solutions calculated with the enhanced Galerkin method. Here $m = 1$ and $n = 15$. Hence, the curve denoted by k is the kth harmonic. Key: ——, exact non-linear model; x x x, quasi-linear model; — — —, spectrally-invariant model. (a) $k = 1$, (b) $k = 2$, (c) $k = 3$.

studies for design by using the system for one set of parameters to quickly find its solution for a similar set of parameters.

Results of computational studies using both digital and analog computers have verified the accuracy of the proposed method and highlighted its unique capabilities. Two example cases were considered. The first example case illustrated the computational method's ability to track both super and subharmonic solution curves for a varying excitation frequency and its ability to significantly reduce the complexity of the problem via order reduction. The second example case, a hydraulic engine mount, demonstrated the solution method's capability to simultaneously handle non-linearities defined in dual domains (time and frequency).

Detailed analysis of an experimental system with a local stiffness non-linearity using the enhanced Galerkin method are documented in a companion article by the same authors [26]. The experimental system is a more complex version of the first example case system considered in this paper and it specifically focuses on the influence of a static load on a local stiffness non-linearity. Also, the non-linear junction is multi-dimensional and many modes of the simply supported beam must be considered. Yet, in another article [27], the semi-analytical strategy introduced here is expanded and applied specifically to an active, non-linear vibration mounting system and the optimal design problem is studied. Stability analysis of systems with local non-linearities using the "enhanced" Galerkin method will be addressed in a future article.

ACKNOWLEDGMENTS

The authors wish to acknowledge the Office of Naval Research Graduate Fellowship Program, the Center for Automotive Research at the Ohio State University, the U.S. Army Research Office (URI Grant DAAL-03-92-G-0120 and the ASSERT Project; Project Monitor: Dr. T. L. Doligalski), and the Ohio State University Graduate School for their financial support. Dr. C. Padmanabhan and Dr. T. E. Rook are also acknowledged for helpful advice and insight into nonlinear systems and computational methods.

REFFERENCES

1. A. H. Nayfeh and D. T. Mook 1979 *Nonlinear Oscillations*. New York: John Wiley.
2. A. Gelb and W. E. Van der Velde 1968 *Multiple Input Describing Functions and Nonlinear System Design*. New York: McGraw Hill.
3. R. J. Comparin and R. Singh 1989 *Journal of Sound and Vibration* **134,** 259–290. Non-linear frequency response characteristics of an impact pair.
4. C. Padmanabhan and R. Singh 1992 *Journal of Sound and Vibration* **155,** 209–230. Spectral coupling issues in a two-degree-of-freedom system with clearance non-linearities.
5. S. L. Lau and Y. K. Cheung 1981 *Transactions of The American Society of Mechanical Engineers*, *Journal of Applied Mechanics* **48,** 959–964. Amplitude incremental variational principle for non-linear vibration of elastic systems.
6. Y. K. Cheung, S. H. Chen and S. L. Lau 1990 *Journal of Sound and Vibration* **140,** 273–86. Application of the incremental harmonic balance method to cubic non-linearity systems.
7. C. Nataraj and H. D. Nelson 1989 *Journal of Sound and Vibration* **111,** 187–93. Period solutions in rotor dynamic systems with non-linear supports: a general approach.
8. A. N. Jean and H. D. Nelson 1990 *Journal of Sound and Vibration* **143,** 473–489. Periodic response investigation of large order non-linear rotordynamic system using collocation.
9. Y. Wang and Z. Wang 1994 *Journal of Sound and Vibration* **177,** 573–576. Periodic response of piecewise-linear oscillators using trigonometric collocation.
10. T. M. Cameron and J. H. Griffin 1989 *Transitions of The American Society of Mechanical Engineers*, *Journal of Applied Mechanics* **56,** 149–54. An alternating frequency/time domain method for calculating the steady-state response of non-linear dynamic systems.
11. Y. B. Kim and S. T. Noah 1991 *Nonlinear Dynamics* **2,** 215–234. Response and bifurcation analysis of a MDOF rotor system with strong nonlinearity.
12. H. S. Choi and J. Y. K. Lou 1991 *International Journal of Nonlinear Mechanics* **26,** 461–473. Nonlinear behavior and chaotic motions of an SDOF system with piecewise-nonlinear stiffness.
13. Y. Ren and C. F. Beards 1994 *Journal of Sound and Vibration* **172,** 593–604. A new receptance-based perturbative multi-harmonic balance method for the calculation of the steady state response of non-linear systems.
14. C. A. J. Fletcher 1984 *Computational Galerkin Methods*. New York: Springer Verlag.
15. M. Urabe and A. Reiter 1966 *Journal of Mathematical Analysis and Applications* **14,** 107–40. Numerical computation of nonlinear forced oscillations by Galerkin's procedure.
16. M. Urabe 1966 *Archives of Rational Mechanical Analysis*, 120–52. Galerkin's procedure for nonlinear periodic systems.
17. T. E. Rook and R. Singh 1995 *Journal of Sound and Vibration* **182,** 303–322. Dynamic analysis of a reverse-idler gear pair with concurrent clearances.
18. E. Brommundt 1974 *Dynamics of Rotors*. On the Numerical Investigation of Nonlinear Periodic Rotor Vibrations. IUTAM Symposium Lyngby, Denmark. Berlin: Springer-Verlag.
19. F. H. Ling and X. X. Wu 1987 *International Journal of Non-linear Mechanics* **22,** 89–98. Fast Galerkin method and its application to determine periodic solutions of non-linear oscillators.
20. C. Padmanabhan and R. Singh 1995 *Journal of Sound and Vibration* **184,** 35–38. Analysis of periodically excited non-linear systems by a parametric continuation technique.
21. G. Kim and R. Singh 1993 *Transactions of the American Society of Mechanical Engineers*, *Journal of Dynamic Systems*, *Measurements*, *and Control* **115,** 482–487. Nonlinear analysis of automotive hydraulic engine mount.
22. G. Kim and R. Singh 1992 *Proceedings of the third ASME Symposium on Transportation Systems*, *Anaheim*, *CA* **DSC-44,** 165–180. Resonance, isolation and shock control characteristics of automotive nonlinear hydraulic engine mounts.
23. G. Kim and R. Singh 1995 *Journal of Sound and Vibration* **179,** 427–53. A study of passive and adaptive hydraulic engine mount systems with emphasis on nonlinear characteristics.
24. J. Pan, J. Pan and C. H. Hansen 1992 *Journal of the Acoustical Society of America* **92,** 895–907. Total power flow from a vibrating rigid body to a thin panel through multiple elastic mounts.
25. Mathworks, Inc. 1994 *MATLAB SIMULINK TOOLBOX Reference Guide*. Natick, Mass.
26. T. J. Royston and R. Singh 1995 *Journal of Sound and Vibration*. Experimental study of a mechanical system containing a local continuous stiffness non-linearity under periodic excitation and a static load.
27. T. J. Royston and R. Singh 1995 *Journal of Sound and Vibration*. Optimization of passive and active non-linear vibration mounting systems based on vibratory power transmission.

APPENDIX A: LIST OF SYMBOLS

A.1. ENHANCED GALERKIN METHOD

$\mathbf{a}_j^x$ jth coefficient vector of the Galerkin solution for $\mathbf{x}$

$\mathbf{F}$ force vector between Sections (A) and (B)

$\mathscr{F}_j$ discrete Fourier transform operator for jth term in series

$\mathscr{F}_j^{-1}$ discrete inverse Fourier transform operator for jth term in series

$\mathbf{D}_j^{x^{mn}}$ jth coefficient vector of the Galerkin method determining equations for $\mathbf{x}^{mn}$-frequency domain form

$\mathbf{d}^{\mathbf{x}}$ vector of second order determining equations for $\mathbf{x}$-time domain form

i $\sqrt{-1}$

Im imaginary part

$\mathbf{J}_\mathbf{a}$ augmented Jacobian

m subharmonic order assumed in Galerkin method

N total number of non-linear algebraic equations for calculation of α

n harmonic order assumed in the Galerkin procedure solution

N_w number of linear degrees-of-freedom and non-linear degrees-of-freedom defined in the frequency domain

N_x number of non-linear degrees-of-freedom defined in the time domain and associated with force inputs

N_y number of degrees-of-freedom connecting Sections (A) and (B)

$\mathbf{Q}$ unitary matrix in QR decomposition

$\mathbf{R}$ upper diagonal matrix in QR decomposition.

R residual error of Galerkin method

Re real part

s iteration index in Figure 3

$\mathbf{T}_\mathbf{y}$ transfer function matrix for Section (B) at the connection point to Section (A)

t time, or iteration index in Figure 3

$\mathbf{V}$ tangent matrix in QR decomposition

$\mathbf{w}$ vector of displacement variables in Section (B)

$\mathbf{x}$ vector of displacement variables in Section (A)

$\mathbf{x}^{mn}$ Galerkin approximation for $\mathbf{x}$ using m subharmonic order and n harmonic order

$\mathbf{y}$ vector of displacement variables connecting Section (A) and Section (B)

$\alpha^{\mathbf{x}}$ array containing coefficient vectors of the Galerkin procedure solution for $\mathbf{x}$

δ Dirac delta function

ϵ tolerance level set for residual R, see Figure 3

τ non-dimensional time variable

ω excitation frequency

ω' arbitrary response frequency

Ω arbitrary system parameter varied in continuation scheme

A.2. EXAMPLE CASE I

A beam cross-sectional area

a^U excitation force coefficient

F_{st} Static excitation force

E beam material modulus of elasticity

I beam moment of inertia

K mount linear stiffness coefficient

l_s beam axial length

M rigid body mass

s axial position on beam

s_b axial position of non-linear element connection point to beam

u beam vertical displacement

δ_{ij} Kronecker delta $-\ \delta_{ij} = 1$ if $i = j$, otherwise $\delta_{ij} = 0$ if $i \neq j$

κ junction cubic stiffness coefficient

ρ beam material density

ξ junction linear damping coefficient

ζ_j beam modal damping ratio

A.3. EXAMPLE CASE II

A hydraulic engine mount inertia track area

a^U excitation force coefficient

A_p hydraulic engine mount equivalent fluid piston area

b_r hydraulic engine mount rubber viscous damping

b_s chassis/suspension linear viscous damping coefficient

I hydraulic mount fluid inertia in inertia track

k_r engine mount rubber stiffness coefficient

k_s chassis/suspension stiffness coefficient

l hydraulic engine mount inertia track length

M_e engine mass

M_s chassis mass

p_{atm} atmospheric pressure
p_1 upper chamber fluid pressure in hydraulic engine mount
p_2 lower chamber fluid pressure in hydraulic engine mount
$\bar{p}$ static equilibrium pressure in hydraulic engine mount
V_{air} air volume trapped in upper chamber of hydraulic engine mount
V_1 hydraulic engine mount upper fluid
V_2 hydraulic engine mount lower fluid chamber volume
v hydraulic engine mount inertia track volume displacement
x_e engine vertical displacement
x_s chassis vertical displacement
λ hydraulic engine mount inertia track resistance parameter
ρ_g hydraulic engine mount fluid density